GRANULAR AVALANCHES ON COMPLEX TOPOGRAPHY

J.M.N.T. GRAY
Institut für Mechanik
Technische Hochschule Darmstadt
64289 Darmstadt, Germany

1. Introduction

The Savage-Hutter theory for the one-dimensional gravity driven free-surface flow of cohesionless granular materials down inclines (Savage & Hutter, 1989) and curved beds (Savage & Hutter, 1991) was generalised to two-dimensions by Hutter *et al.* (1992) and Greve *et al.* (1994). Savage & Hutter (1991) introduced a simple curvilinear coordinate system Oxz with the x coordinate parallel to, and the z component normal to, the local one-dimensional chute geometry. In the two-dimensional theories a similar coordinate system $Oxyz$ was adopted with a lateral (or cross slope) coordinate y perpendicular to the x, z coordinates. Thus, the curvilinear surface $z = 0$ followed a quasi one-dimensional chute topography, with down slope but no cross slope variation. Agreement between experiments performed on such a chute and the predicted two-dimensional spreading of these unconfined granular avalanches was extremely good (Koch *et al.*, 1994). Recently the theory has been generalised (Gray *et al.*, 1996) to allow for *shallow* down and cross slope variation in the basal chute geometry. In this paper a comparison is made between the theoretical predictions and experimental results from two chutes with complex down and cross slope topography.

2. Governing equations

In the Savage-Hutter theory the avalanche is treated as an incompressible granular material satisfying a Mohr-Coulomb constitutive relation with internal angle of friction ϕ. The kinematic free surface is traction free and at the base the avalanche slides on a rigid impenetrable basal topography. A Coulomb-type rate-independent dry friction law, with basal friction angle δ, is used to model the *slip* at the base of the avalanche. The simple

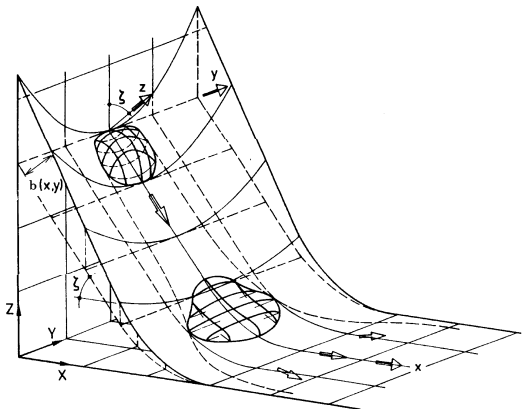

Figure 1. The simple curvilinear coordinate system $Oxyz$ consists of an inclined plane connected to a horizontal plane by a smooth transition. The local inclination angle of the curvilinear surface $z = 0$ (dashed lines) is ζ. The actual basal topography $z = b(x, y)$ (solid lines) is superposed to top of the $z = 0$ curvilinear surface.

curvilinear coordinate system $Oxyz$ introduced in §1 is adopted here, however, following Gray *et al.* (1996) the $z = 0$ curvilinear surface no longer represents the basal topography. Instead the actual chute geometry is prescribed by defining its height $b(x, y)$ above the curvilinear surface $z = 0$. The curvilinear coordinate system (dashed lines) and the *superposed* basal topography (solid lines) is illustrated in Figure 1. For notational purposes we shall continue to refer to x as the down slope and y as the cross slope directions, respectively, even though the physical downslope direction may no longer be in the x direction. Extensive use is made of the fact that the avalanche and the basal geometry are shallow. That is the typical downslope length scale for order unity changes in the avalanche and the basal geometry are much greater than their heights. This together with the fact that the down and cross slope velocity components are nearly independent of depth allows the mass and momentum equations to be integrated through the avalanche depth to remove one space dimension.

The depth integrated mass balance reduces to

$$\frac{dh}{dt} + h\left(\frac{\partial u}{\partial x} + \frac{\partial v}{\partial y}\right) = 0, \tag{1}$$

where h is the avalanche thickness and u, v are the downslope and cross slope components of the velocity $\boldsymbol{v}$. The leading order depth integrated

momentum balances reduce to

$$\left.\begin{aligned} \frac{du}{dt} &= g\sin\zeta - \frac{u}{|\boldsymbol{v}|}\tan\delta(g\cos\zeta + \kappa u^2) - g\cos\zeta\left(K_x\frac{\partial h}{\partial x} + \frac{\partial b}{\partial x}\right), \\ \frac{dv}{dt} &= \qquad - \frac{v}{|\boldsymbol{v}|}\tan\delta(g\cos\zeta + \kappa u^2) - g\cos\zeta\left(K_y\frac{\partial h}{\partial y} + \frac{\partial b}{\partial y}\right), \end{aligned}\right\} \tag{2}$$

where g is the gravitational acceleration, ζ, $\kappa = -\partial\zeta/\partial x$ are the local inclination angle and the local curvature of the curvilinear surface $z = 0$ and K_x, K_y are earth pressure coefficients. The essential difference between these equations and those of Greve *et al.* (1994) are the basal topography gradients $\partial b/\partial x$ and $\partial b/\partial y$ on the right-hand side of (2). The remaining terms on the right-hand side are the gravity acceleration, the basal friction and the earth pressure terms that arise from the stress divergence.

The earth pressures, which relate the *limiting* stresses normal and parallel to the inclined plane, were introduced by Savage & Hutter (1989) and subsequently generalised to two-dimensions by Hutter *et al.* (1992). The earth pressure coefficients are either *active*, or *passive*, depending on whether the motion is dilatational, or compressional

$$K_x = \begin{cases} K_{x_{act}} & \partial u/\partial x > 0, \\ K_{x_{pas}} & \partial u/\partial x < 0, \end{cases} \tag{3}$$

$$K_y = \begin{cases} K_{y_{act}}^{x_{act}} & \partial u/\partial x > 0, \quad \partial v/\partial y > 0, \\ K_{y_{act}}^{x_{pas}} & \partial u/\partial x < 0, \quad \partial v/\partial y > 0, \\ K_{y_{pas}}^{x_{act}} & \partial u/\partial x > 0, \quad \partial v/\partial y < 0, \\ K_{y_{pas}}^{x_{pas}} & \partial u/\partial x < 0, \quad \partial v/\partial y < 0. \end{cases} \tag{4}$$

Their values are given by

$$K_{x_{act/pas}} = 2\sec^2\phi\left(1 \mp \{1 - \cos^2\phi\sec^2\delta\}^{1/2}\right) - 1, \tag{5}$$

$$K_{y_{act/pas}}^{x} = \frac{1}{2}\left(K_x + 1 \mp \{(K_x - 1)^2 + 4\tan^2\delta\}^{1/2}\right), \tag{6}$$

and it is easy to show that $K_{x_{act}} \leq K_{x_{pas}}$ and $K_{y_{act}}^{x_{act}} \leq K_{y_{act}}^{x_{pas}} \leq K_{y_{pas}}^{x_{act}} \leq K_{y_{pas}}^{x_{pas}}$. That is the active earth pressure coefficients are always less than the passive earth pressure coefficients.

3. Comparison between experiment and theoretical predictions

Laboratory experiments have been performed on two chutes in order to validate the theory. The first geometry (V02) has a shallow concave parabolic cross slope profile on the inclined section of the chute and broadens out into a flat horizontal plane (Fig. 2a). The second topography (ISO3)

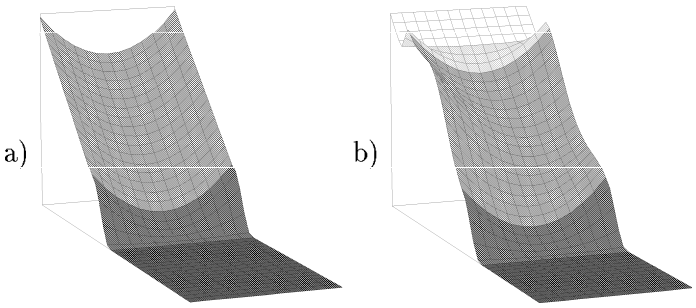

Figure 2. The basal chute geometry used in the experiments and numerical computations: a) symmetric parabolic chute (V02), b) the snaking valley chute (ISO3). The shading highlights the different zones in the respective chutes.

consists of an inclined flat plane, which narrows into a shallow parabolic channel that has an additional shallow *snaking valley* topography in the x-direction, before once again broadening out into the horizontal plane (Fig. 2b). The snaking valley is achieved by a sinusoidal down slope shift of the cross slope parabolic profile.

TABLE 1. Material parameters and chute geometry

Experiment	V02	ISO3
Bed friction angle, δ	30°	29°
Internal angle of friction, ϕ	40°	35°
Chute inclination, ζ	40°	40°
Channel radius of curvature, R	110 cm	85 cm
Amplitude of sinusoid	0 cm	20 cm
Cap radius, r_c	32 cm	18 cm
Cap height, h_c	22 cm	18 cm

Numerous laboratory experiments have been performed on both chutes. In this paper we describe only one experiment, on each of the chutes, that is representative of the general characteristics of the flow. The chute geometry and the properties of the granular materials are summarised in Table 1. Typical run times are of the order of 1.5-2 seconds for V02 and 2-2.5 seconds for experiment IS03. The flowing avalanche is recorded on video and high speed camera. This allows the avalanche edge to be determined at a series of time steps. Two experimental parameters are required for the theoretical predictions: the granular material's internal angle of friction ϕ and the bed friction angle δ. The internal angle of friction is determined by measuring

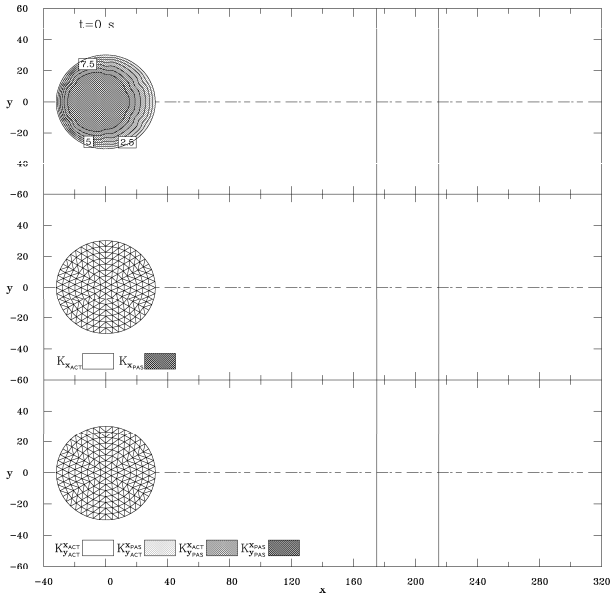

Figure 3. The initial configuration of experiment V02 is illustrated in three panels using projected curvilinear coordinates (x, y). The avalanche runs from left to right and all lengths are in cm. The solid lines at $x = 175$ and $x = 215$ cm indicate the position of the transition zone between the 40° inclined parabolic section to the left and the horizontal plane to the right of the chute. The dashed line along $y = 0$ indicates the Talweg. The top panel shows the avalanche thickness (in cm), the middle panel the downslope earth pressure and the bottom panel the cross slope earth pressure. The active/passive earth pressure states are indicated by shading the elements, a key is given on the plot. The time is indicated in the top left corner.

the steepest angle of inclination of a conical pile of the granular material. Whilst the basal angle of friction is measured by tilting a planar section of the bed topography and measuring the angle at which a static sample of the granular material begins to slide.

A Lagrangian explicit finite difference scheme is used to solve the system of equations (1)–(6). This has been developed by Wieland *et al.* (1996) and is based on the original one-dimensional method of Savage & Hutter (1989). The avalanche is initially discretised into a finite number of triangular elements. It follows from the thickness continuity equation (1) and Reynolds Transport theorem that the initial volume of granular material contained in each of the elements is preserved throughout the flow. At each time-step the algorithm then proceeds as follows, (1) the new positions of the element corners are computed by an explicit forward step in time, (2) the area of the new triangle is computed, (3) the thickness of the element is then determined by dividing the initial element volume by its current area, (4) the new velocity is then computed by an explicit step in time. The grid

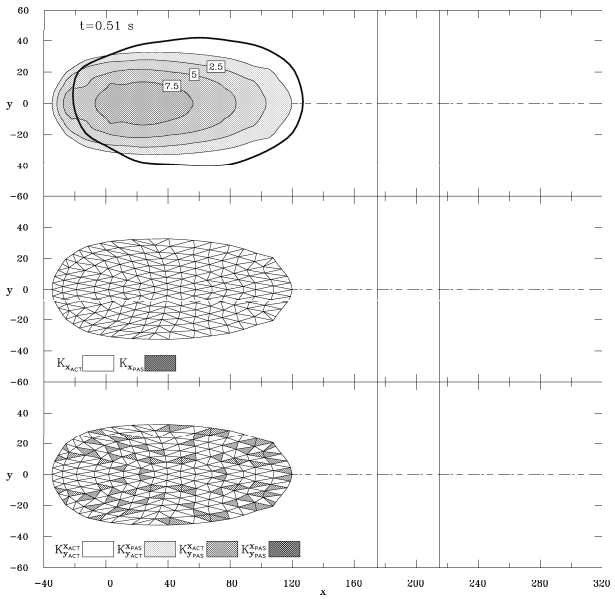

Figure 4. The same as Fig. 3. The thick line in the top panel indicates the experimentally determined position of the avalanche edge.

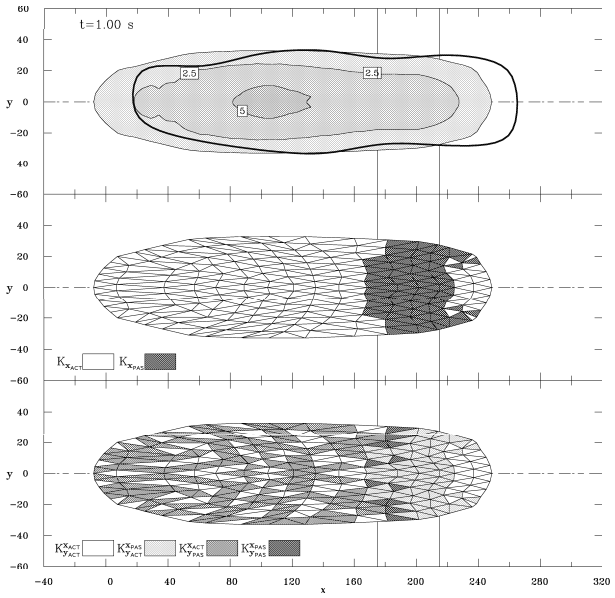

Figure 5. The same as Fig. 3. The thick line in the top panel indicates the experimentally determined position of the avalanche edge.

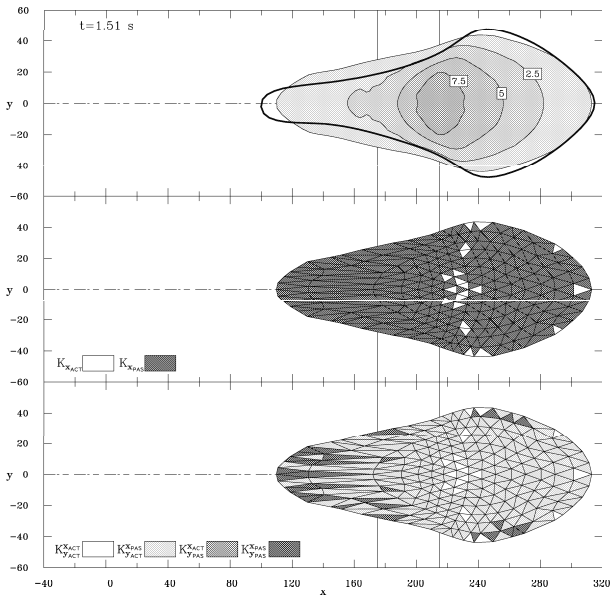

Figure 6. The same as Fig. 3. The thick line in the top panel indicates the experimentally determined position of the avalanche edge.

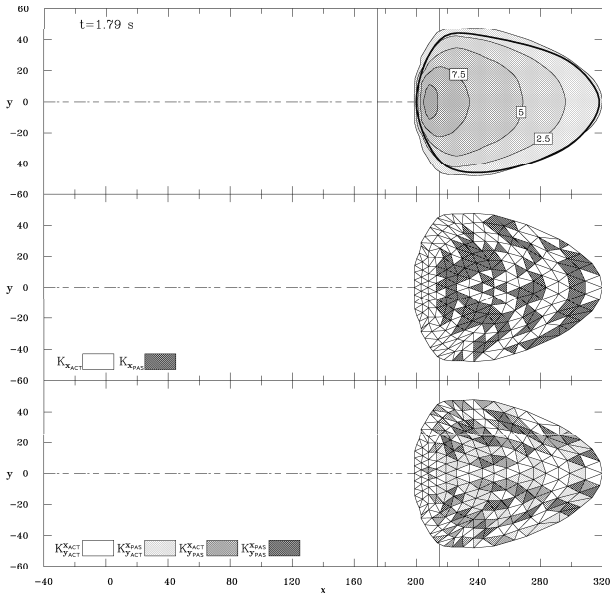

Figure 7. The same as Fig. 3. The thick line in the top panel indicates the experimentally determined position of the avalanche edge.

mesh therefore moves and deforms with the avalanche.

The predicted avalanche flow on the parabolic chute (V02) and comparison with the experimentally determined avalanche edge is shown in the sequence of figures 3–7. Each of the figures is divided into three panels showing the thickness, the down slope, and the cross slope earth pressures from top to bottom, respectively. The predicted flow of V02 is symmetric about the Talweg (the line joining the lowest points in the valley) as expected. As the cap is released (Fig. 3) the avalanche expands rapidly in the down-slope direction reducing in thickness correspondingly. In the cross-slope direction there is an initial expansion followed by convergence, as the thickness gradients reduce, and the geometry is able to channel the flow (Fig. 4). As the granular material enters into the transition zone (Fig. 5) the down slope earth pressure switches immediately from active to passive. And, as it proceeds into the horizontal run-out zone (Fig. 6) it compresses in the down-slope direction and expands laterally, giving it a *tadpole* structure with a pronounced nose and tail. Finally, Figure 7 shows the predicted position of the granular material when the avalanche has come to rest, this is in extremely good agreement with the experimental results. During the flowing phase of the predicted avalanche the tail section has a tendency to move somewhat slower than the experiments suggest. This can be compensated for by linearly reducing the bed friction angle along the avalanche length. A physical explanation for this phenomenon is that the bed friction is not rate-independent (as assumed here) and some additional velocity dependent Voellmy-type drag is required. The experimental results are quite sensitive to the bed-friction angle, but not as sensitive to the internal angle of friction. Larger bed friction angles imply that the avalanche moves more slowly and stops much faster in the run-out zone. In some cases the bed friction angle was high enough to bring the granular material to rest whilst still on the inclined section of the chute.

The second experiment (ISO3) is illustrated in the sequence of figures 8–13. The avalanche is initiated on an inclined plane (Fig. 8) and spreads far more rapidly than in V02, which was partially confined in the parabolic channel. The rapid spreading is in agreement with the initial phases of the experiments of Koch *et al.* (1994) on quasi one-dimensional surfaces. However, as soon as the granular material enters into the valley section (Fig. 9) it is strongly channelised in the cross-slope direction and *steered* by the topography (Fig. 10). The stress state as indicated by the earth pressure coefficients is extremely sensitive to the geometry of the chute. As it enters the run-out zone (Fig. 11) there is strong down-slope convergence and cross-slope spreading again giving it a nose and tail like tadpole structure. Figure 12 shows the position of the predicted avalanche at the time that the real avalanche comes to rest. Again we see that the tail moves

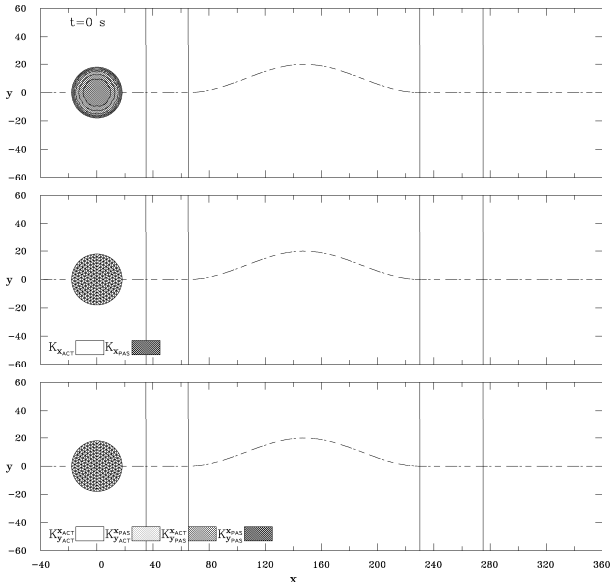

Figure 8. The same as Fig. 3 except for experiment ISO3. Initially the granular material is released on a 40° inclined plane. The lines at x = 35, 65, 230, 275 cm indicate the position of the transition zones between the inclined plane, the sinusoidal snaking valley and the horizontal plane. The dashed line shows the position of the Talweg.

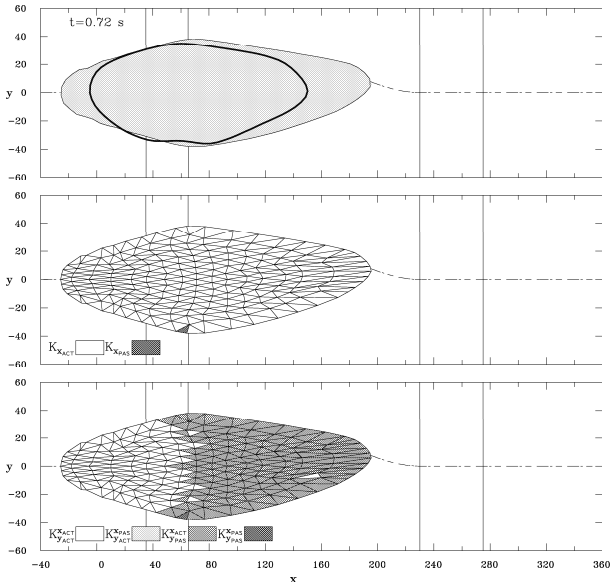

Figure 9. The same as Fig. 8. The thick line in the top panel indicates the experimentally determined position of the avalanche edge.

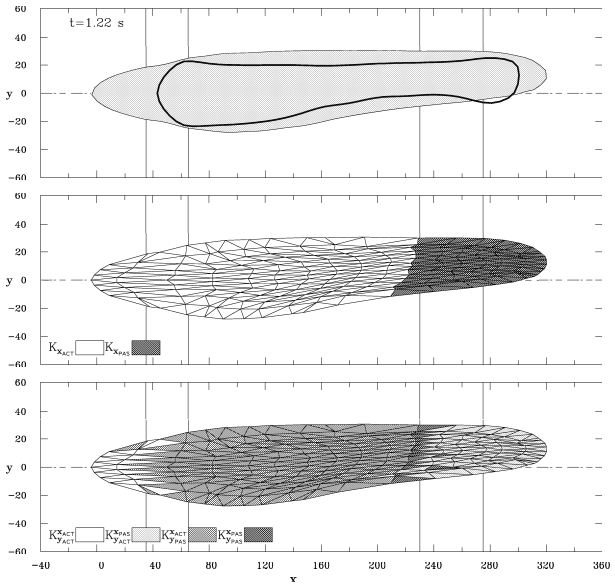

Figure 10. The same as Fig. 8. The thick line in the top panel indicates the experimentally determined position of the avalanche edge.

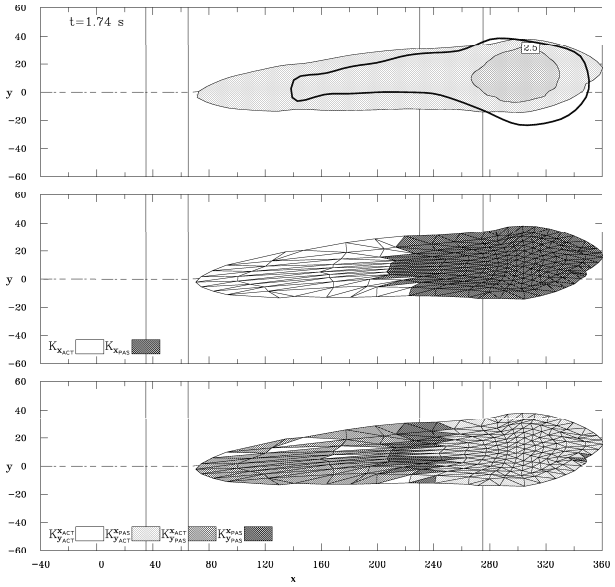

Figure 11. The same as Fig. 8. The thick line in the top panel indicates the experimentally determined position of the avalanche edge.

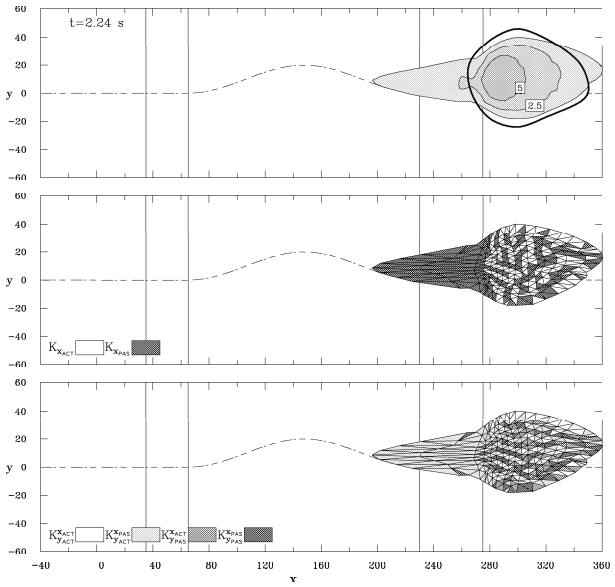

Figure 12. The same as Fig. 8. The thick line in the top panel indicates the experimentally determined position of the avalanche edge.

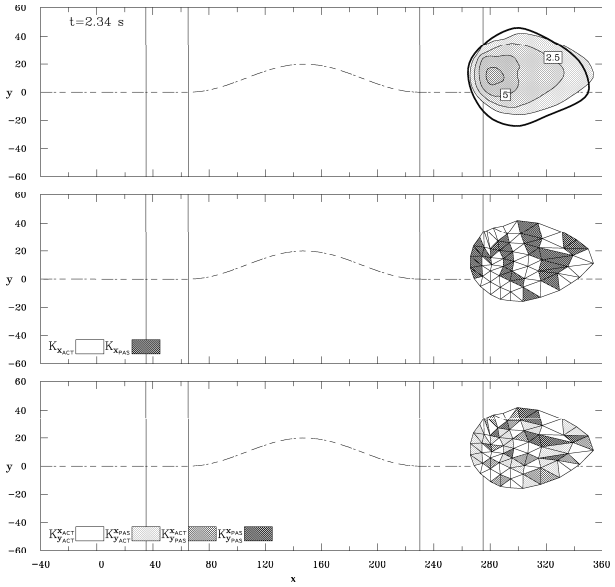

Figure 13. The same as Fig. 8. The thick line in the top panel indicates the experimentally determined position of the avalanche edge.

somewhat too slowly, however, a tenth of a second later in figure 13 the computed avalanche has also come to rest and the position of the deposit is in extremely good agreement with experiment. The centre of the resulting pile of avalanched material was positioned on the side towards which the avalanche was initially guided. This was because in the initial stages of the motion, when the avalanche velocity was relatively small, the geometry played a greater role than in the latter stages, when the momentum is high enough to overcome the steering effect.

4. Discussion

The Savage-Hutter theory has been extended to allow the flow of granular avalanches to be modelled on shallow downslope and cross slope topography (Gray *et al.*, 1996). In this paper we have demonstrated that there is extremely good agreement between the theory and laboratory experiments on two chutes with complex geometry. However, we have also encountered some numerical difficulties with the algorithm of Wieland *et al.* (1996) when there is rapid convergence of the granular material. In particular the fine mesh computation illustrated in figure 12 becomes numerically unstable shortly after $t = 2.24$ s, and the picture of the final deposit (Fig. 13) was produced by using a courser mesh. Improvement of the numerical algorithm is a major thrust of our current research efforts.

This research was supported by the Deutsche Forschungsgemeinschaft SFB 298 project "Deformation und Versagen bei metallischen und granularen Strukturen". Dr Gray would like to acknowledge the invaluable assistance of Herr Wall and Herr Tai in conducting the experiments.

References

Gray, J.M.N.T., Wieland, M. and Hutter, K. (in prep) Channelised free surface flow of a cohesionless granular avalanche in a chute with shallow lateral curvature. Part I: theory.

Greve, R., Koch, T. and Hutter, K. (1994) Unconfined flow of granular avalanches along a partly curved surface. Part I: Theory. *Proc. R. Soc. A*, **445**, 399-413.

Koch, T., Greve, R. and Hutter, K. (1994) Unconfined flow of granular avalanches along a partly curved surface, Part II: Experiments and numerical computations. *Proc. R. Soc. A*, **445**, 415-435.

Hutter, K. Siegel, M. Savage, S.B. and Nohguchi, Y. (1992) Two-dimensional spreading of a granular avalanche down an inclined plane Part I. Theory. *Acta Mech.*, **100**, 37-68.

Savage, S. B. and Hutter, K. (1989) The motion of a finite mass of granular material down a rough incline. *J. Fluid Mech.*, **199**, 177-215.

Savage, S. B. and Hutter, K. (1991) The dynamics of avalanches of granular materials from initiation to runout. Part I: Analysis. *Acta Mech.*, *86*, 201-223.

Wieland, M. Gray, J.M.N.T. and Hutter, K. (in prep) Channelised free surface flow of a cohesionless granular avalanche in a chute with shallow lateral curvature. Part II: Numerical predictions and comparison with experiments.